Journal of Materials Chemistry A

ROYAL SOCIETY OF CHEMISTRY

PAPER

View Article Online
View Journal | View Issue

Cite this: J. Mater. Chem. A, 2025, 13, 19374

Influence of methyl substitution on linear diboronic acids: toward spiroborate covalent organic framework formation in *N*,*N*-diethylformamide†

Xue Wang,[ab] Qiang Zhu,[ab] Hang Qu,[b] Xiang Zhou,[b] Mounib Bahri,[c] Bowen Liu,[b] Thomas Fellowes,[ab] Rob Clowes,[b] Hongjun Niu,[b] Nigel D. Browning[c] and Andrew I. Cooper *[ab]

Received 20th March 2025
Accepted 20th May 2025

DOI: 10.1039/d5ta02297e

rsc.li/materials-a

Recently, we reported the reconstruction of two-dimensional (2D) to three-dimensional (3D) covalent organic frameworks (COFs) *via* base-catalyzed boronate ester to spiroborate linkage conversion. In that work, we tentatively attributed the interlayer close-packing in the 2D **BPDA-COF** as the main cause for the long reaction time—40 days—required to complete the structure reconstruction in *N*,*N*-diethylformamide (DEF). Here, we address this hypothesis by designing methyl-substituted 4,4′-biphenyldiboronic acid (BPDA) with large molecular twist to weaken the packing between boronate esters. Experiments show that the spiroborate COF formation is accelerated by increased molecular twist in three linear diboronic acids linkers, with the pure 3D spiroborate phase obtained in 3 days *via* reaction of Co(II) 2,3,9,10,16,17,23,24-octahydroxyphthalocyaninato ($(OH)_8$PcCo) in *N*,*N*-diethylformamide (DEF). Mechanistic studies reveal that methyl-substituted linear diboronic acids are more liable to protodeboronation, which also contributes to the accelerated spiroborate structure formation.

Introduction

Covalent organic frameworks (COFs) have been explored for applications such as gas adsorption, catalysis, and energy storage.[1] Boron, with the electronic configuration $[He]2s^2 2p^1$, generally undergoes sp^2 or sp^3 hybridization to adopt trigonal planar or tetrahedral geometries, respectively, though rare examples of sp hybridization exist.[2,3] In the field of COFs, the sp^2 and sp^3 hybridized boron are typically represented by neutral boronate ester[4] and anionic tetraoxyborate[5,6] or spiroborate linkage.[7,8] According to our recent study, a 2D boronate ester COF—**BPDA-COF**—can be reconstructed to a 3D spiroborate COF—**SPB-COF-DEA**—under basic environments.[9,10] When employing neat *N*,*N*-diethylformamide (DEF) as the solvent and reacting at 120 °C, 40 days are required to complete this structural transformation. Mechanistic studies have suggested a boronate ester to spiroborate linkage conversion *via* base-catalyzed boronate ester protodeboronation.[10] According to the literature, the prehydrolysis of boronate ester to boronic acid is the rate determining step for this reaction.[11] In prior reports, Dichtel *et al.* have discovered that the more closely-packed 2D boronate ester COFs exhibit improved hydrolytic stability because of the increased energy barriers to interlayer exfoliation and monomer release.[12] Based on our mechanistic studies and the results of Dichtel *et al.*, we have tentatively assumed that it is the interlayer close-packing in 2D **BPDA-COF** that protected the boronate esters from hydrolysis, which then required 40 days to transform the 2D boronate ester COF to a pure 3D spiroborate COF in DEF. Here, we test this hypothesis by weakening the interlayer packing of 2D boronate ester COFs and explore its influence toward spiroborate COFs formation.

It is known that employing monomers of good planarity can enhance interlayer π–π stacking and facilitate the crystallization of 2D layered COFs.[12,13] For example, 2D honeycomb-type COF with planar triazine core has showed much improved crystallinity and shortened interlayer d-spacing (3.49 Å) as compared to the structure analogue with a non-planar triphenylamine core (4.0 Å).[14] Conversely, introducing twisted precursors usually results in diminished interlayer interactions that prevents effective packing between layers, as exemplified when highly twisted hexaazatrinaphthylene nodes (twisted-HATNA)[15] or chiral 1,1′-bi-2-naphthol (BINOL) linker[16] is employed for 2D-layered COFs synthesis. In either scenario, molecular twists are sterically enforced by rigid, bulky substitutions. According to these reports, we assume that by judicious precursor molecular conformation design, like, internal

[a]Leverhulme Research Centre for Functional Materials Design, University of Liverpool, Liverpool, L7 3NY, UK. E-mail: aicooper@liverpool.ac.uk

[b]Department of Chemistry and Materials Innovation Factory, University of Liverpool, Liverpool, L69 7ZD, UK

[c]Albert Crewe Centre for Electron Microscopy, University of Liverpool, Liverpool, L69 3GL, UK

† Electronic supplementary information (ESI) available. See DOI: https://doi.org/10.1039/d5ta02297e

molecular twist introduction *via* substitutions, we can weaken or disrupt the interlayer packing of 2D **BPDA-COF**.

Specifically, **BPDA-COF** has been synthesized from the condensation between Co(II) 2,3,9,10,16,17,23,24-octahydroxyphthalocyaninato ($(OH)_8$PcCo) and 4,4′-biphenyldiboronic acid (BPDA).[10] In **BPDA-COF**, although the square Co(II) phthalocyanine (CoPc) ring with large aromatic domain is the major contributing part to the interlayer tight packing, structural modification of CoPc unit is synthetically challenging. We therefore propose to modulate the interlayer packing of **BPDA-COF** *via* twist introduction to the linear diboronic acid—**BPDA**.

By introducing two or four methyl substitutions at the 2,2′ or 2,2′,6,6′ positions on 4,4′-biphenyldiboronic acid (**BPDA**), we obtained two new linear diboronic acids, namely **BPDA-2** and **BPDA-4** (Fig. 1a). A survey of the known single crystal structures in the Cambridge Structural Database (CSD) revealed that the dihedral angle of biphenyl unit is 0–60° in linker **BPDA**, 60–90° in **BPDA-2** and 80–90° in **BPDA-4**, suggesting increased molecular twist in order in the three linkers (Fig. S9†). Condensations of $(OH)_8$PcCo with linker **BPDA**, **BPDA-2** and **BPDA-4** afforded **BPDA-COF**, **BPDA-2-COF** and **BPDA-4-COF** of 2D boronate ester structure, mixed 2D boronate ester and 3D spiroborate, and pure 3D spiroborate structure, respectively (Fig. 1). The corresponding COF structures was confirmed by a set of characterizations including powder X-ray diffraction (PXRD), Fourier-transform infrared (FTIR) spectroscopy and solid-state nuclear magnetic resonance (NMR). Mechanistic studies indicated that methyl-substituted **BPDA-2** and **BPDA-4** are more liable to protodeboronation, as compared to **BPDA**, which also contributes to the accelerated spiroborate COF formation.

Results and discussion

Synthesis and characterization of COFs

Linker **BPDA-2** and **BPDA-4** were synthesized from their corresponding amino precursors *via* a three-step procedure that involving Sandmeyer reaction to convert amino group to bromine, followed by Miyaura borylation and a subsequent boronate ester hydrolysis to give boronic acids. The amino precursor of **BPDA-4** was synthesized from the reduction of 3, 5-dimethylnitrobenzene to obtain 1,2-bis(3,5-dimethylphenyl) hydrazine and a follow-up acid catalysed benzidine rearrangement (ESI†).[17] Solvothermal condensation of $(OH)_8$PcCo with linker **BPDA**, **BPDA-2** and **BPDA-4** in DEF at 120 °C for 3 days yielded **BPDA-COF**, **BPDA-2-COF** and **BPDA-4-COF**, respectively (Fig. 1a).

Experimental PXRD characterizations of the three COFs exhibited multiple well-defined diffraction peaks, suggesting high periodicity in two/three dimension (Fig. 1b–d). The experimental PXRD pattern of **BPDA-COF** was consistent with the reported 2D boronate ester crystal model of **sql** topology in AA-stacking mode, showing diffraction peaks at 3.26, 4.67, 6.60, 9.88, 13.15 and 16.52°, which were assigned to (100), (110), (200), (300), (400) and (430) planes. Pawley refinement confirmed a tetragonal lattice with unit cell parameters (a = 26.913(9) Å, c = 3.590(9) Å) (Fig. 1b).[9,10] PXRD of **BPDA-4-COF** closely resembled our previously reported 3D spiroborate COF of non-interpenetrated **nbo** topology, indicating the formation of a pure spiroborate phase in **BPDA-4-COF**.[8,10] **BPDA-4-COF** showed diffraction peaks at 3.62, 5.13, 7.23, 8.08, 10.25, 10.85, 11.47, 13.09, 14.73, 18.16, 20.67 and 23.29°, which were indexed as (110), (200), (220), (310), (400), (330), (420), (510), (530), (550), (811) and (910) planes, respectively. Pawley refinement yielded a cubic I centered lattice with unit cell parameters of a = 34.724(6) Å (Fig. 1d). By contrast, the PXRD of **BPDA-2-COF** resembled the combined patterns of **BPDA-COF** and **BPDA-4-COF**, indicating a mixed phase of 2D boronate ester and 3D spiroborate structures (Fig. 1c). Specifically, in **BPDA-2-COF**, diffractions at 3.36, 4.75 and 6.76° can be assigned to the (100), (110) and (200) planes of the corresponding 2D boronate ester crystal model of **sql** topology in AA-stacking mode. Pawley refinement confirmed a tetragonal lattice with unit cell parameters of a = 26.091(2) Å, c = 3.814(4) Å. Diffraction peaks at 3.60, 5.10, 7.22, 8.08, 10.22, 10.85, 11.42, 13.04, 14.49, 14.93, 16.19, 18.15, 18.50, 20.55 and 23.30° were indexed as (110), (200), (220), (310), (400), (330), (420), (510), (440), (530), (620), (710), (640), (800) and (910) planes of the 3D spiroborate structure, respectively. Pawley refinement yielded a cubic I centered lattice with unit cell parameters of a = 34.513(5) Å. Comparing this result with our prior study, while the formation of a pure 3D spiroborate COF from linker **BPDA** in DEF takes 40 days,[10] here, the spiroborate COF formation was accelerated by reacting $(OH)_8$PcCo with methyl-substituted **BPDA-2** and **BPDA-4**. Typically, when **BPDA-4** was employed as the linker, a pure spiroborate phase can be isolated after 3 days.

To gain insight into the type of linkage that was formed in the three COFs, model reactions were conducted by reacting catechol with the three linkers under COF synthesis condition. Notably, we observed that while the reaction between catechol and **BPDA** in DEF afforded pink-white coloured crystal precipitates, the reaction of catechol with **BPDA-2** or **BPDA-4** resulted in a homogeneous solution in brown colour. Solution ^{1}H NMR analysis of the crystal precipitates confirmed a boronate ester product—**m-BE-BPDA**—in 56.4% yield, consistent with the boronate ester structure in **BPDA-COF** (Fig. 2a). Characterization of the isolated powder products from the reaction of catechol with **BPDA-2** or **BPDA-4** by solution ^{1}H, ^{13}C and ^{11}B NMR identified a spiroborate structure—**m-SPB-DEA**, with the spiroborate linkage and the $[NH_2Et_2]^+$ counter cations been validated by the single crystal structure of **m-SPB-DEA** (Fig. 2a and b). LC-MS analysis of the reaction mixture of catechol with **BPDA-2** and **BPDA-4** observed 2,2′-dimethyl-1,1′-biphenyl and 2,2′,6,6′-tetramethylbiphenyl as the reaction by-products, respectively (Fig. S8†). The results from model compound study were broadly the same as the result of COFs. While the reaction between catechol and linker **BPDA-2** afforded solely **m-SPB-DEA** with spiroborate structure, we suppose the interlayer packing of the formed boronate esters protected the structure integrity of the boronate ester phase in **BPDA-2-COF**.

The chemical structure of the three COFs was further characterized by FTIR, solid-state carbon-13 cross-polarization/magic angle spinning NMR (^{13}C CP/MAS NMR) and boron-11 magic angle spinning NMR (^{11}B MAS NMR) spectroscopy. Like the three linkers, FTIR spectra of **m-BE-BPDA** and **BPDA-COF**

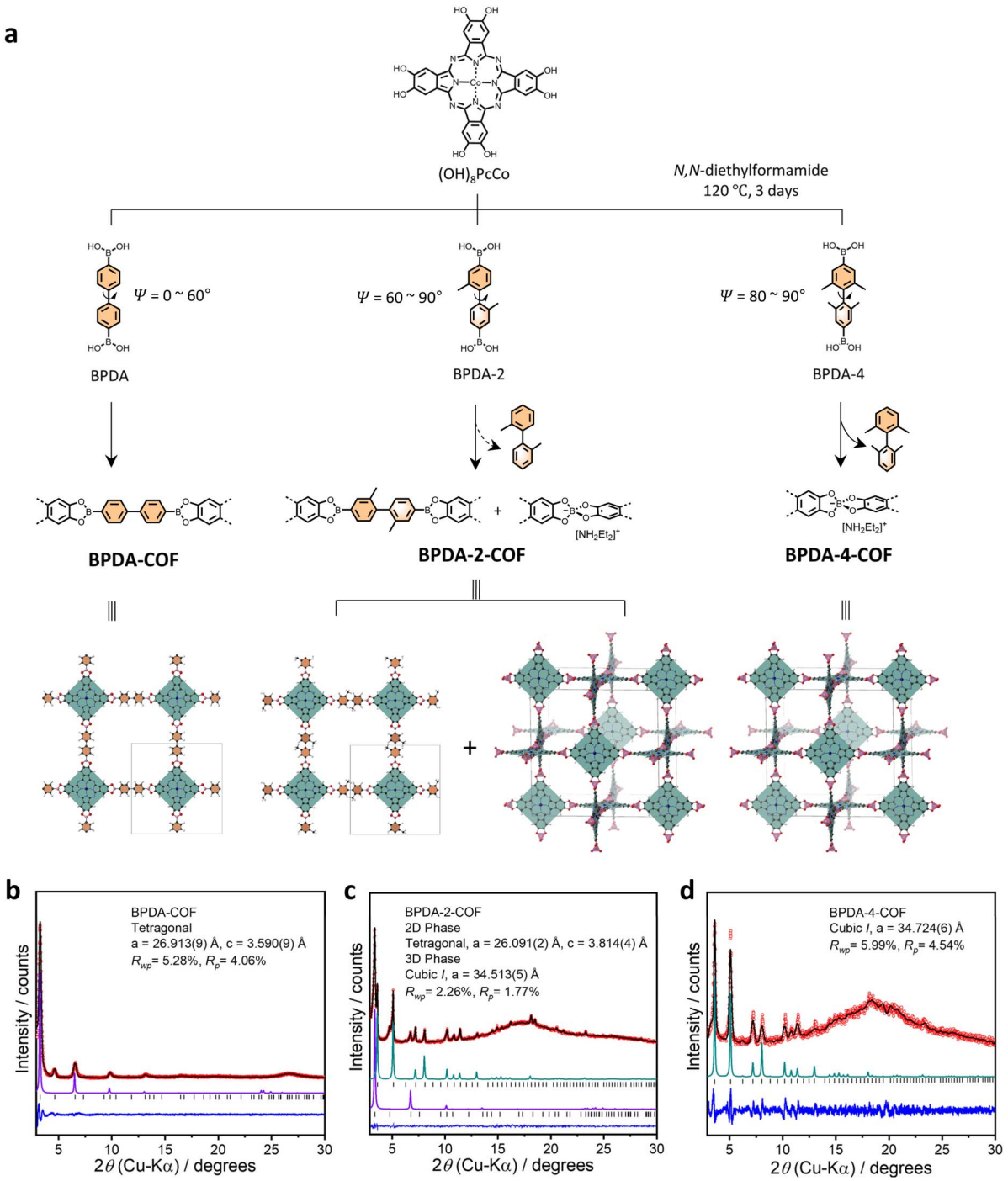

Fig. 1 (a) Scheme for the synthesis of BPDA-COF, BPDA-2-COF and BPDA-4-COF with graph representations of their corresponding crystal models. The pink tetrahedra represents the spiroborate linkage and gray lines indicate the unit cell. Experimental PXRD pattern (red), profile calculated from Pawley fitting (black) showing the residual (blue), compared with the pattern simulated from the structural model (purple and green) for as-synthesized (b) BPDA-COF, (c) BPDA-2-COF and (d) BPDA-4-COF. Reflection positions are shown by tick marks.

showed a strong absorption band between 1329–1331 cm^{-1}, corresponding to the stretching vibrations of the B–O of the trigonal [-BO_2]. While FTIR spectra of **BPDA-2-COF** and **BPDA-4-COF** were consistent with the spectrum of **m-SPB-DEA**, showing characteristic B–O stretching vibrations of $[BO_4]^-$ tetrahedral at ~1045 cm^{-1} (Fig. S11 and S12†).[10] FTIR results corroborated the boronate ester structure of **BPDA-COF** and the formation of spiroborate linkage in **BPDA-2-COF** and **BPDA-4-COF**. In the solid-state ^{13}C CP/MAS NMR spectra of the three COFs, signals between 154.9 and 95.8 ppm corresponding to phthalocyanine carbons were identified. The carbon signal at 16.6 ppm in **BPDA-2-COF** corresponded to methyl carbon in linker **BPDA-2**,

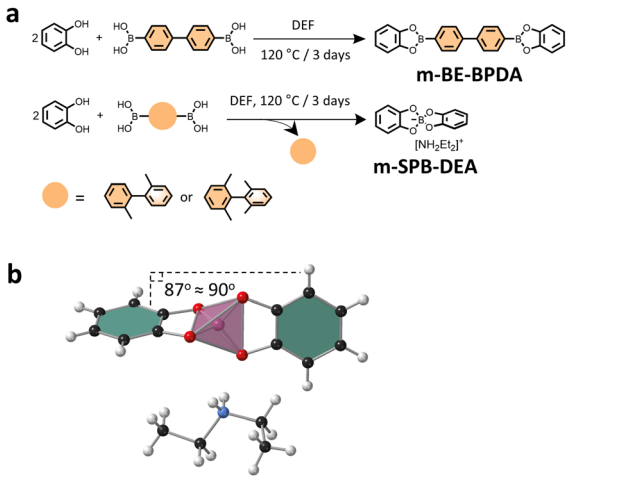

Fig. 2 (a) Scheme for the synthesis of the model compounds. (b) Single crystal structure of **m-SPB-DEA**. The pink tetrahedron represents spiroborate linkage.

while the carbon signals at 42.2 and 12.3 ppm in **BPDA-2-COF**, at 43.6 and 13.7 ppm in **BPDA-4-COF** were assigned to the secondary and primary carbons in the ethyl group of $[NH_2Et_2]^+$ counter cation (Fig. S13–15†).[8,10] Solid-state ^{11}B MAS NMR spectra of **BPDA-COF** and **BPDA-4-COF** showed a single signal at 19.96 and 11.41 ppm, consistent with the same 2D boronate ester and 3D spiroborate COF reported before.[10] **BPDA-2-COF** exhibited a single signal at 16.16 ppm in ^{11}B NMR spectrum, suggesting a mixed boronate ester and spiroborate linkage (Fig. S16†). The thermal stability of the three COFs was investigated by thermogravimetric analysis (TGA) (Fig. S17†). TGA curve of **BPDA-COF** showed around 5% weight loss at 500 °C and another 35% weight loss when heated up to 950 °C under N_2 atmosphere. TGA analysis of **BPDA-4-COF** revealed about 10% weight loss at 200 °C, which corresponds to the loss of guest molecules (*e.g.*, H_2O, DEF).[18,19] The 20% weight loss between 200–450 °C was possibly from the loss of $[NH_2Et_2]^+$ cation in the COF pores,[20,21] and the 20% weight loss above 450 °C may arise from the decomposition of the COF.[22] TGA curve of **BPDA-2-COF** was similar to **BPDA-4-COF** but with slightly higher thermal stability.

The porosity of the three COFs was evaluated by nitrogen sorption measurements at 77 K (Fig. 3a–c). The Brunauer–Emmett–Teller (BET) surface areas were calculated to be 1269, 1529 and 1246 $m^2\ g^{-1}$ for **BPDA-COF**, **BPDA-2-COF** and **BPDA-4-COF**. By fitting the density functional theory (DFT) model to the N_2 isotherm, the derived pore size distribution (PSD) was found to be centred at 2.45 and 3.02 nm for **BPDA-COF** and **BPDA-4-COF**, supporting the 2D boronate ester structure of **BPDA-COF** and the 3D spiroborate structure of **BPDA-4-COF**.[10] PSD of **BPDA-2-COF** revealed dual pores located at 2.13 and 3.10 nm, which corresponds to the 2D boronate ester and 3D spiroborate phase in **BPDA-2-COF**, respectively. The higher BET surface area of **BPDA-2-COF** than **BPDA-4-COF** was possibly due to the higher crystallinity of the sprioborate phase in **BPDA-2-COF**.

Scanning electron microscopy (SEM) images of the 2D **BPDA-COF** showed an overall flower-like morphology assembled from multiple rods (Fig. 3d). While the literature have shown that SEM images of the same spiroborate COF can have uniform cubic morphology,[8] SEM image of **BPDA-4-COF** revealed small particles with particle size of ~100 nm (Fig. 3f). SEM image of **BPDA-2-COF** showed a mixed morphology of rods and cubes (Fig. 3e). By comparing with the SEM image of the 2D **BPDA-COF** and the 3D spiroborate COF, we attributed the rod-like morphology to the 2D boronate ester phase and the cubes to the 3D spiroborate phase. However, transmission electron microscope (TEM) analysis of **BPDA-2-COF** revealed that both the cubes and the rods corresponds to the 3D spiroborate phase (Fig. 3g–i). Specifically, fast fourier transform (FFT) of the cubes clarified d-spacing of 2.35 and 1.69 nm, corresponding to (110) and (200) planes of the 3D spiroborate COF model. While the identified d-spacing of 2.38 nm of the rods can be assigned to the (110) plane of the 3D spiroborate phase. We did not observe the 2D phase from our TEM measurements. TEM images of **BPDA-COF** showed crystalline domains with identified d-spacing of 2.70 nm, corresponding to the (100) plane of the proposed 2D boronate ester structure model. TEM test for the crystalline structure of **BPDA-4-COF** was unsuccessful (Fig. S24–S26†).

Mechanistic study

Regarding the spiroborate structure formation in **BPDA-2-COF** and **BPDA-4-COF**, one potential route is *via* boronate ester to spiroborate linkage conversion.[10] This route involves the pre-hydrolysis of the formed boronate esters to liberate the corresponding diol and boronic acid. Under basic environments, boronic acids undergo protodeboronation to release anionic $[B(OH)_4]^-$,[11,23] which will react with diols to form spiroborate structures (Fig. 4a). In this study, we observed that the methyl-substituted linker **BPDA-2** and **BPDA-4** were capable to release anionic $[B(OH)_4]^-$ in DEF as the previously reported linker **BPDA**.[10] Specifically, after subjecting **BPDA-2** and **BPDA-4** to DEF at 120 °C for 3 days, ^{11}B NMR spectra of their reaction mixture showed one broad signal at ~20.00 ppm and a sharp peak at 1.48 ppm, corresponding to the sp^2 hybridized boron in boric acid ($B(OH)_3$) and the sp^3 hybridized boron in anionic $[B(OH)_4]^-$, respectively (Fig. 4b).[10] LC-MS analysis of the reaction mixtures detected 2,2′-dimethyl-1,1′-biphenyl (from **BPDA-2**) and 2,2′,6,6′-tetramethyl-1,1′-biphenyl (from **BPDA-4**) as the reaction by-products, respectively, confirming protodeboronation occurred (Fig. S28†). This result obtained is in good agreement with the previous report and supported the feasibility of spiroborate structure formation in **BPDA-2-COF** and **BPDA-4-COF** *via* a linkage conversion way.

If we consider that methyl-substitutions onto linker **BPDA** only introduce steric effects to interfere with the effective packing between formed boronate esters and assuming the linkage conversion from boronate ester the only route to form spiroborate structure, then the above results support our initial assumption that the spiroborate COF formation can be accelerated by weakening or disrupting the packing of boronate

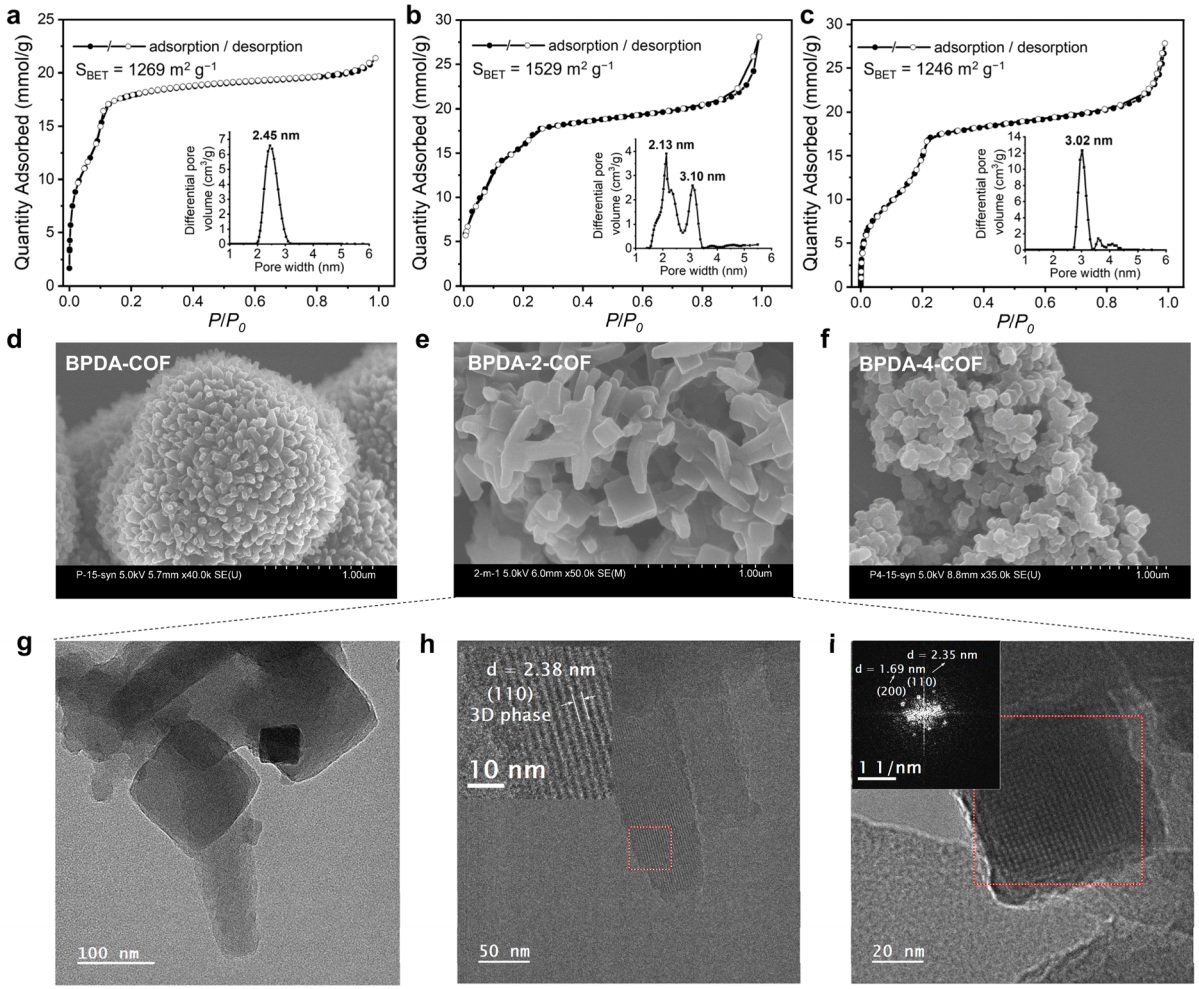

Fig. 3 N_2 sorption isotherms and the corresponding pore size distribution (PSD) profiles were calculated from DFT, and SEM images of (a and d) **BPDA-COF**, (b and e) **BPDA-2-COF** and (c and f) **BPDA-4-COF** were shown. (g–i) TEM images of **BPDA-2-COF**. The rod-shaped and cube-shaped morphologies were characterized respectively. Inset of (i) is the Fast Fourier Transform (FFT) of the area within red frame in (i).

esters. If this is the case, the accelerated spiroborate COF formation in **BPDA-2-COF** and **BPDA-4-COF** is due to the promoted monomer release—the hydrolysis step in Fig. 4a (step 1).

However, further characterizations indicate that methyl-substitutions onto the linker **BPDA** also contribute to the accelerated spiroborate COF formation by promoting the protodeboronation of linear diboronic acids (step 2 in Fig. 4a) – that is, the reactivity of the linker is affected. While we did not observe the signal of $B(OH)_3$ in the solution ^{11}B NMR spectrum of **BPDA**, ^{11}B NMR spectra of linker **BPDA-2** and **BPDA-4** showed a weak signal at ~20.00 ppm, suggesting protodeboronation occurred at room temperature in dmso-d_6 (Fig. 4c). In addition, LC-MS test of the reaction mixture of linkers in neutral condition (1,4-dioxane : methanol = 2 : 1, v/v) revealed that the concentration of protodeboronation by-product from linker **BPDA-2** (2,2′-dimethyl-1,1′-biphenyl) was higher than **BPDA** (biphenyl) (Fig. S31†), though both samples were prepared at a concentration of 1 mg. mL^{-1}. These results together suggest that **BPDA-2** and **BPDA-4** are more liable to protodeboronation than **BPDA**. Such methyl substitution promoted protodeboronation of boronic acids is consistent with literature conclusions that electron-donating groups like methyl groups can increase protodeboronation liability of arylboronic acids.[24]

Based on these data, we propose that the accelerated spiroborate COF formation by reacting $(OH)_8PcCo$ with methyl-substituted **BPDA-2** and **BPDA-4** is due to a synergistic effect of the weakened or disrupted packing between the formed boronate esters that promoted the release of boronic acids and, the increased protodeboronation liability of boronic acids by methyl substitutions. Depending on the rate of boronate ester formation and the protodeboronation of dibornic acid linker, the protodeboronation of the linker may happen independently prior to boronate ester formation. Taking the synthesis of **BPDA-2-COF** as an example, on the one hand, as compared to 2D **BPDA-COF**, the employment of the twisted **BPDA-2** weakened the interlayer packing of the formed boronate esters, which can facilitate boronate ester hydrolysis to release boronic acids (step 1 in Fig. 4a). On the other hand, methyl-substituted **BPDA-2** is more prone to protodeboronation than **BPDA** to

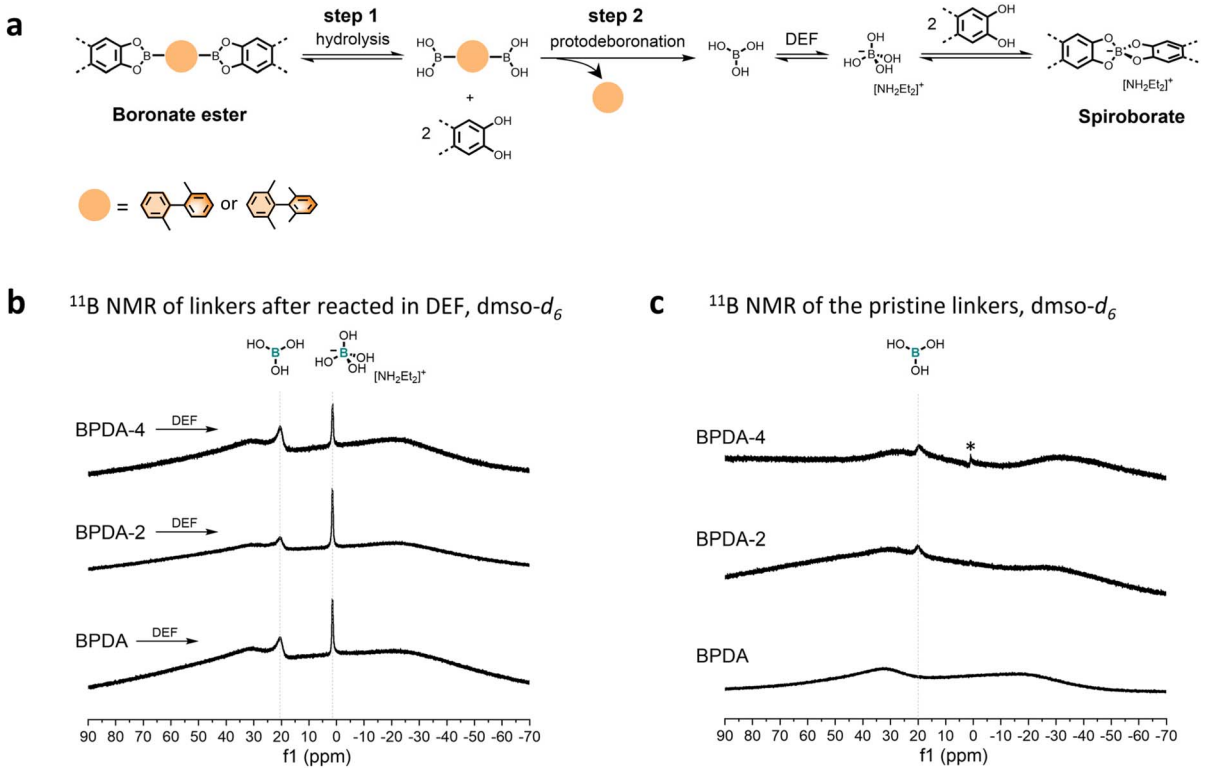

Fig. 4 (a) Proposed scheme for spiroborate structure formation. (b) Solution ^{11}B NMR of linker **BPDA**, **BPDA-2** and **BPDA-4** after reacted in DEF at 120 °C for 3 days. (c) Solution ^{11}B NMR of pristine **BPDA**, **BPDA-2** and **BPDA-4**. *The weak, sharp signal at ~1.0 ppm in the ^{11}B NMR spectra of linker **BPDA-4** can be assigned to tetrahydroxyborate ion. Solution ^{11}B NMR were conducted in quartz NMR tube.

release $B(OH)_3$ to form anionic $[B(OH)_4]^-$ for the formation of spiroborate structures in DEF (step 2 in Fig. 4a). These two factors together contribute to the accelerated spiroborate structure formation in **BPDA-2-COF**. This explains why a pure spiroborate phase can be achieved in 3 days when employing **BPDA-4** as the linker, as **BPDA-4** shows the largest molecular twist that can effectively prohibit the packing between boronate esters.

Conclusions

In this work, the introduction of two or four methyl substitutions to 4,4′-biphenyldiboronic acid (**BPDA**) increases the precursor molecular twist, accelerating spiroborate COF formation in DEF. By reacting $(OH)_8$PcCo with the three linkers **BPDA**, **BPDA-2** and **BPDA-4** with sequentially increased molecular twists, we realize accelerated spiroborate COF formation in order of the degree of twist. Mechanistic studies indicate that methyl substitution also contributes to the accelerated spiroborate COF formation in a way of promoting the protodeboronation liability of boronic acid. This work deepens our understanding toward boron chemistry in COF chemistry and can potentially inspire further research on exploring the protodeboronation mechanism of methyl-substituted aryl boronic acids.

Data availability

The data that support the findings of this study are presented in the paper and the ESI.†

Author contributions

The manuscript was written through contributions of all authors. All authors have given approval to the final version of the manuscript.

Conflicts of interest

There are no conflicts to declare.

Acknowledgements

For funding, the authors acknowledge the Leverhulme Trust *via* the Leverhulme Research Centre for Functional Materials Design and the Engineering and Physical Sciences Research Council (EPSRC) (EP/V026887/1). X. Wang thanks Yushu Han for the help on processing the sorption data. This project has received funding from the European Research Council under the European Union's Horizon 2020 research and innovation program (grant agreement no. 856405).

Notes and references

1 M. S. Lohse and T. Bein, Covalent Organic Frameworks: Structures, Synthesis, and Applications, *Adv. Funct. Mater.*, 2018, **28**(33), 1705553.
2 H. Braunschweig, R. D. Dewhurst, K. Hammond, J. Mies, K. Radacki and A. Vargas, Ambient-Temperature Isolation of a Compound with a Boron-Boron Triple Bond, *Science*, 2012, **336**(6087), 1420–1422.
3 H. Braunschweig, T. Dellermann, R. D. Dewhurst, B. Hupp, T. Kramer, J. D. Mattock, J. Mies, A. K. Phukan, A. Steffen and A. Vargas, Strongly Phosphorescent Transition Metal π-Complexes of Boron–Boron Triple Bonds, *J. Am. Chem. Soc.*, 2017, **139**(13), 4887–4893.
4 A. P. Côté, A. I. Benin, N. W. Ockwig, M. O'Keeffe, A. J. Matzger and O. M. Yaghi, Porous, Crystalline, Covalent Organic Frameworks, *Science*, 2005, **310**(5751), 1166–1170.
5 Y. Hu, B. Sengupta, H. Long, L. J. Wayment, R. Ciora, Y. Jin, J. Wu, Z. Lei, K. Friedman, H. Chen, *et al.*, Molecular recognition with resolution below 0.2 angstroms through thermoregulatory oscillations in covalent organic frameworks, *Science*, 2024, **384**(6703), 1441–1447.
6 D. Asgari, J. Grüneberg, Y. Luo, H. Küçükkeçeci, S. Ghosh, V. Chevelkov, S. Fischer-Lang, J. Roeser, A. Lange, B. Dunn, *et al.*, An anionic two dimensional covalent organic framework from tetratopic borate centres pillared by lithium ions, *Nat. Commun.*, 2024, **15**(1), 7031.
7 Y. Du, H. Yang, J. M. Whiteley, S. Wan, Y. Jin, S.-H. Lee and W. Zhang, Ionic Covalent Organic Frameworks with Spiroborate Linkage, *Angew. Chem., Int. Ed.*, 2016, **55**(5), 1737–1741.
8 X. Wang, M. Bahri, Z. Fu, M. A. Little, L. Liu, H. Niu, N. D. Browning, S. Y. Chong, L. Chen, J. W. Ward, *et al.*, A Cubic 3D Covalent Organic Framework with nbo Topology, *J. Am. Chem. Soc.*, 2021, **143**(37), 15011–15016.
9 V. S. P. K. Neti, X. Wu, M. Hosseini, R. A. Bernal, S. Deng and L. Echegoyen, Synthesis of a phthalocyanine 2D covalent organic framework, *CrystEngComm*, 2013, **15**(36), 7157–7160.
10 X. Wang, T. Fellowes, M. Bahri, H. Qu, B. Li, H. Niu, N. D. Browning, W. Zhang, J. W. Ward and A. I. Cooper, 2D to 3D Reconstruction of Boron-Linked Covalent–Organic Frameworks, *J. Am. Chem. Soc.*, 2024, **146**(20), 14128–14135.
11 H. L. D. Hayes, R. Wei, M. Assante, K. J. Geogheghan, N. Jin, S. Tomasi, G. Noonan, A. G. Leach and G. C. Lloyd-Jones, Protodeboronation of (Hetero)Arylboronic Esters: Direct *versus* Prehydrolytic Pathways and Self-/Auto-Catalysis, *J. Am. Chem. Soc.*, 2021, **143**(36), 14814–14826.
12 B. J. Smith, N. Hwang, A. D. Chavez, J. L. Novotney and W. R. Dichtel, Growth rates and water stability of 2D boronate ester covalent organic frameworks, *Chem. Commun.*, 2015, **51**(35), 7532–7535.
13 M. Martínez-Abadía and A. Mateo-Alonso, Structural Approaches to Control Interlayer Interactions in 2D Covalent Organic Frameworks, *Adv. Mater.*, 2020, **32**(40), 2002366.
14 J. Dong, Y. Wang, G. Liu, Y. Cheng and D. Zhao, Isoreticular covalent organic frameworks for hydrocarbon uptake and separation: the important role of monomer planarity, *CrystEngComm*, 2017, **19**(33), 4899–4904.
15 A. B. Marco, D. Cortizo-Lacalle, I. Perez-Miqueo, G. Valenti, A. Boni, J. Plas, K. Strutyński, S. De Feyter, F. Paolucci, M. Montes, *et al.*, Twisted Aromatic Frameworks: Readily Exfoliable and Solution-Processable Two-Dimensional Conjugated Microporous Polymers, *Angew. Chem., Int. Ed.*, 2017, **56**(24), 6946–6951.
16 X. Wu, X. Han, Q. Xu, Y. Liu, C. Yuan, S. Yang, Y. Liu, J. Jiang and Y. Cui, Chiral BINOL-Based Covalent Organic Frameworks for Enantioselective Sensing, *J. Am. Chem. Soc.*, 2019, **141**(17), 7081–7089.
17 I. Yonekawa, K. Mutoh, Y. Kobayashi and J. Abe, Structurally and electronically modulated spin interaction of transient biradicals in two photon-gated stepwise photochromism, *Photochem. Photobiol. Sci.*, 2018, **17**(3), 290–301.
18 D. Saha and S. Deng, Synthesis, characterization and hydrogen adsorption in mixed crystals of MOF-5 and MOF-177, *Int. J. Hydrogen Energy*, 2009, **34**(6), 2670–2678.
19 S. Hausdorf, W. Seichter, E. Weber and F. O. R. L. Mertens, Large pores generated by the combination of different inorganic units in a zinc hydroxide ethynylene diisophthalate MOF, *Dalton Trans.*, 2009, (7), 1107–1113.
20 N. Saffon-Merceron, M.-C. Barthélémy, C. Laurent, I. Fabing, P. Hoffmann and A. Vigroux, An Unusual 3D Zinc-Organic Framework Constructed from Paddle-Wheel-Based Carboxylate Sheets Bridged by Acetate Ions, *Z. Anorg. Allg. Chem.*, 2016, **642**(11), 709–713.
21 M. Mączka, A. Gągor, J. Hanuza, A. Pikul and M. Drozd, Synthesis and characterization of two novel chiral-type formate frameworks templated by protonated diethylamine and ammonium cations, *J. Solid State Chem.*, 2017, **245**, 23–29.
22 R. Seoudi, G. S. El-Bahy and Z. A. El Sayed, FTIR, TGA and DC electrical conductivity studies of phthalocyanine and its complexes, *J. Mol. Struct.*, 2005, **753**(1), 119–126.
23 P. A. Cox, M. Reid, A. G. Leach, A. D. Campbell, E. J. King and G. C. Lloyd-Jones, Base-Catalyzed Aryl-B(OH)$_2$ Protodeboronation Revisited: From Concerted Proton Transfer to Liberation of a Transient Aryl Anion, *J. Am. Chem. Soc.*, 2017, **139**(37), 13156–13165.
24 S.-J. Ahn, C.-Y. Lee, N.-K. Kim and C.-H. Cheon, Metal-Free Protodeboronation of Electron-Rich Arene Boronic Acids and Its Application to ortho-Functionalization of Electron-Rich Arenes Using a Boronic Acid as a Blocking Group, *J. Org. Chem.*, 2014, **79**(16), 7277–7285.